PHYSICAL REVIEW B VOLUME 21, NUMBER 8 15 APRIL 1980

Neutron-diffraction study of the static structure factor and pair correlations in liquid ^{4}He

E. C. Svensson, V. F. Sears, A. D. B. Woods,* and P. Martel
Atomic Energy of Canada Limited Research Company, Chalk River, Ontario, Canada KOJ 1JO
(Received 3 December 1979)

An investigation of the structure of liquid ^{4}He at saturated vapor pressure by means of neutron diffraction is reported for 11 temperatures in the range 1.00 to 4.27 K. At each temperature, the static structure factor $S(Q)$ is obtained for $0.8 \leq Q \leq 10.8$ Å^{-1} with an average statistical precision of 0.8% and with a residual systematic error which is estimated to be $<1\%$. Our results for $S(Q)$ are in good agreement with the very precise x-ray results of Hallock which cover the range $0.133 \leq Q \leq 1.125$ Å^{-1} and with the requirement that the corresponding pair correlation functions $g(r)$, which we obtain from $S(Q)$ by Fourier inversion, vanish inside the core of the interatomic potential. The temperature variations of both $S(Q)$ and $g(r)$ show clearly that the degree of spatial order in liquid ^{4}He increases with decreasing temperature above the λ point, 2.17 K, but then decreases with decreasing temperature in the superfluid phase. The latter behavior is believed to be a consequence of the Bose-Einstein condensation. A comparison of our results for $S(Q)$ and $g(r)$ at 1.00 K with the results of theoretical calculations for $T = 0$ reveals significant discrepancies which indicate that there is a greater degree of spatial order in liquid ^{4}He than would be the case if the atoms interacted via additive forces of the Lennard-Jones type.

I. INTRODUCTION

The static structure factor $S(Q)$ and the corresponding pair correlation function $g(r)$ of liquid ^{4}He have been extensively studied over the past 40 years by both x-ray-diffraction[1-12] and neutron-diffraction[13-17] experiments, and the qualitative behavior of these quantities has been reasonably well established. However, the quantitative accuracy of the results is not, in general, sufficient to satisfy present requirements for several different applications. One notable exception is the very precise small-angle x-ray-scattering results of Hallock[12] which, however, cover only a very limited range of wave vectors, $0.133 \leq Q \leq 1.125$ Å^{-1}. In addition, there appear to be serious discrepancies among many of the published values. For example, there exist discrepancies among the reported values of the height of the main peak of $S(Q)$ of 16% near the λ point and of 12% at lower temperatures.

One obvious need for accurate experimental $S(Q)$ and $g(r)$ values is for the testing of theories. In recent years there have been many theoretical calculations of $S(Q)$ and $g(r)$ for liquid ^{4}He at $T = 0$. Most of these calculations have been based on the use of variational wave functions of the Jastrow type.[18-29] More recently, results have also been obtained by direct Monte Carlo integration of the Schrödinger equation[26,30] and by the use of Green's-function techniques.[31] A limited number of theoretical results is also available for finite temperatures.[31,32] The quality of the results obtained from the more recent theoretical calculations is now sufficiently high that the existing experimental values for $S(Q)$ and $g(r)$ are no longer accurate enough to provide critical tests or incentive for further improvements to the theories.

Accurate values of the static structure factor $S(Q)$ are also required for normalization purposes in experiments to determine the dynamic structure factor $S(Q, \omega)$ by means of neutron inelastic scattering. An accurate absolute normalization of $S(Q, \omega)$ is especially necessary if one wishes to determine the effective pair potential in liquid ^{4}He from an analysis of the frequency moments of the experimentally determined $S(Q, \omega)$. The lack of accurate experimental values for $S(Q)$ certainly hindered the attempt[33] to determine the effective pair potential in this way.

A method was suggested some years ago[34,35] for the experimental determination of the condensate fraction n_0 in superfluid ^{4}He from the temperature variation of $g(r)$ at large r. Once more, the values for $g(r)$ obtained from existing x-ray- and neutron-diffraction measurements were found[35,36] to be too inaccurate to provide a critical test of the method or to yield very precise values for n_0.

In view of the above considerations, we undertook a program to determine $S(Q)$ for liquid ^{4}He at saturated vapor pressure over a wide range of Q values with considerably higher accuracy and at a larger number of temperatures than had been done previously and, subsequently, to obtain, by Fourier inversion, correspondingly accurate $g(r)$ values. In this paper we present the results of this study and give a comparison with available theoretical calculations.

To determine $S(Q)$ accurately by means of neutron-diffraction measurements, the raw data

must, in general, be corrected for empty-cassette scattering, fast-neutron background, various absorption and shielding effects, multiple scattering, order contamination in the incident neutron beam, inelastic scattering, variations in the detector efficiency, incoherent scattering, and instrumental resolution. The results must also, of course, be properly normalized. In the case of x-ray diffraction the correction for inelastic scattering is negligible but this advantage is offset by the existence of other corrections, such as for Compton scattering and the atomic form factor, which are not present for neutron diffraction. In general, x-ray scattering is at a disadvantage at large Q where the falloff in intensity caused by the atomic form factor precludes accurate structure-factor measurements. On the other hand, accurate neutron-diffraction measurements are difficult at small Q owing to the large background intensities which result from the combined effects of the large beam areas (typically 5×5 cm^2) and the small scattering angles. The discrepancies among the previous $S(Q)$ results are, we believe, due more to differences in the treatment of the necessary corrections than to any basic disagreement among the measurements themselves. The statistical accuracy was also quite poor in many cases.

The high accuracy achieved in the present study is due, in part, to improvements in the prescriptions for making the above corrections and to the availability of a modern high-speed computer which allowed these prescriptions to be carried out satisfactorily. A large amount of spectrometer time (about three months) was also needed to accumulate data which combine high statistical precision with high instrumental resolution over a wide range of wave vectors for several temperatures. In total we have determined $S(Q)$ for $0.8 \leq Q \leq 10.8$ Å^{-1} at temperatures of 1.00, 1.38, 1.77, 1.97, 2.07, 2.12, 2.15, 2.27, 3.00, 3.60, and 4.27 K with an average statistical precision of 0.8% and with a residual systematic error which is estimated to be less than 1%.

Liquid ^{4}He has a number of advantages over other simple liquids as far as the determination of $S(Q)$ by neutron diffraction is concerned. Firstly, ^{4}He has ideal neutron properties, since it is a totally coherent scatterer with zero absorption at thermal-neutron energies. Secondly, the large zero-point motion resulting from the very light mass reduces the density of liquid ^{4}He to a point where it is structurally more closely analogous to a dense gas than to an ordinary liquid. As a result, the oscillations in $S(Q)$ have small amplitudes which decrease rapidly with increasing Q so that the large-Q limit of $S(Q)$ can readily be reached. This enables one to obtain a very accurate normalization and, at the same time, avoid the truncation problems which, for other liquids, complicate the Fourier analysis required to determine $g(r)$ from $S(Q)$. In the present study we have, for the first time for any liquid, effectively reached the infinite-Q limit since, to within the accuracy of our results which extend to $Q = 10.8$ Å^{-1}, the oscillations have died out beyond $Q \simeq 6$ Å^{-1}.

As a combined result of the high specific volume of liquid ^{4}He ($\simeq$46 Å^3/atom) and the small scattering cross section (1.1 b/atom), the neutron mean free path is very large ($\simeq$42 cm). This allows one to use a cylindrical specimen having a diameter (4.44 cm in our experiments) comparable to the full beam width and still have high transmission ($\simeq$92%) and hence low multiple scattering ($\simeq$1%). The advantage of cylindrical geometry is that the shielding factors are, for all practical purposes, independent of the scattering angle and, together with the multiple scattering, easily calculable. For other liquids, high neutron utilization (which requires a large specimen area) and high transmission can be achieved only with slab geometry for which the above corrections are much more complicated.

The only disadvantage of liquid ^{4}He is the small atomic mass as a result of which the correction for inelastic scattering (i.e., the Placzek correction) is very large at the largest angles of scattering (as much as $\simeq$50% in the present study). The conventional method for making this correction is not applicable to ^{4}He so that we have found it necessary to develop an alternative method which is described in Sec. II together with the other background material.

Details of the experiment are presented in Sec. III and of the data analysis in Sec. IV. The results for $S(Q)$ are given in Sec. V and the corresponding results for $g(r)$ in Sec. VI. These results are then compared with available theoretical calculations in Sec. VII, and some closing remarks are made in Sec. VIII.

II. THEORY

The double-differential scattering cross section, which describes the scattering of a neutron of mass m_n by a monatomic system of N atoms from an initial state with wave vector $\vec{k}$ and energy $\hbar\epsilon = (\hbar k)^2/2m_n$ to a final state with wave vector $\vec{k}'$ and energy $\hbar\epsilon'$, is given by[37]

$$\frac{d^2\sigma}{d\Omega d\epsilon'} = Nb^2 \frac{k'}{k} S(Q, \omega), \tag{1}$$

where b is the bound scattering length and $S(Q, \omega)$

denotes the dynamic structure factor. Here $\vec{Q}=\vec{k}-\vec{k}'$ and $\omega=\epsilon-\epsilon'$ are the momentum and energy (in units of $\hbar$) transferred from the neutron to the system in the collision and for a liquid $S(Q,\omega)$ is, as indicated, independent of the direction of $\vec{Q}$.

In the present paper the quantity of primary interest is the static structure factor,

$$S(Q)=\int_{-\infty}^{\infty}S(Q,\omega)d\omega, \tag{2}$$

from which one can obtain the pair correlation function $g(r)$ for the liquid via the relationship

$$g(r)=1+(2\pi^2\rho r)^{-1}\int_0^{\infty}Q[S(Q)-1]\sin Qr\,dQ, \tag{3}$$

where ρ is the number density.

In principle, $S(Q)$ could be determined experimentally from Eq. (2) using the dynamic structure factor obtained from neutron-inelastic-scattering experiments. However, in practice, $S(Q)$ can be determined more accurately from a "diffraction" experiment in which one measures the angular distribution of the scattered neutrons without energy analysis. Apart from corrections mentioned in the Introduction and discussed in detail in Sec. IV, the observed scattering is then proportional to the effective differential scattering cross section,

$$\left(\frac{d\sigma}{d\Omega}\right)_{\text{eff}}=\int_0^{\infty}\eta(\epsilon')\frac{d^2\sigma}{d\Omega\,d\epsilon'}d\epsilon', \tag{4}$$

where $\eta(\epsilon')$ is the detector efficiency. It then follows from Eq. (1) that

$$\left(\frac{d\sigma}{d\Omega}\right)_{\text{eff}}=Nb^2\chi(\epsilon,\varphi), \tag{5}$$

where ϕ is the scattering angle and

$$\chi(\epsilon,\phi)=\int_{-\infty}^{\epsilon}\eta(\epsilon-\omega)\left(1-\frac{\omega}{\epsilon}\right)^{1/2}S(Q(\omega),\omega)d\omega, \tag{6}$$

in which

$$Q(\omega)=k[2-\omega/\epsilon-2\cos\phi(1-\omega/\epsilon)^{1/2}]^{1/2}. \tag{7}$$

$Q(\omega)$ curves for the conditions of the present experimental study are shown in Fig. 1 for various values of ϕ.

If the scattering were elastic, so that

$$S(Q,\omega)=S(Q)\delta(\omega), \tag{8}$$

it would then follow from Eq. (6) that

$$\chi(\epsilon,\phi)=\eta(\epsilon)S(Q_0), \tag{9}$$

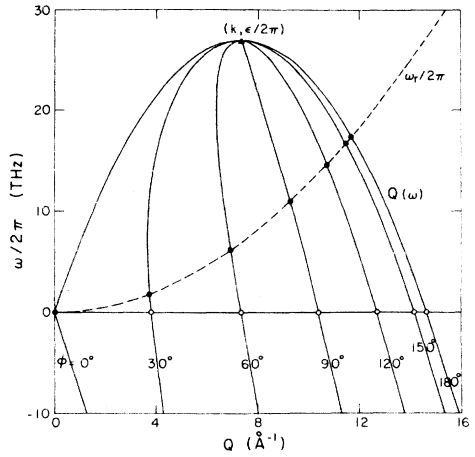

FIG. 1. Kinematics of neutron diffraction in liquid ^{4}He for the conditions of the present measurements. For a given scattering angle ϕ, the scattered neutrons follow the corresponding $Q(\omega)$ curve as shown above for selected ϕ values. The static wave vectors, $Q_0=Q(0)$, are represented by the open circles and the corrected wave vectors $Q(\omega_r)$ by the filled circles.

where $Q_0=Q(0)$, so that

$$Q_0=2k\sin(\phi/2). \tag{10}$$

Although the scattering from a liquid is never strictly elastic, the expressions (8) and hence (9) are often good approximations for heavy atoms.

In general, the integral (6) can be evaluated[38] by first expanding the integrand in powers of ω and then using the moment relations for $S(Q_0,\omega)$. In this way one obtains the familiar Placzek expansion[39] in which the leading term gives the static approximation, (9), and the remaining terms represent the inelastic scattering correction. The latter constitute an expansion in powers of $1/A$, where A is the atom-to-neutron mass ratio. This expansion is rapidly convergent for many liquids but not for liquid ^{4}He where $A\simeq 4$. For light atoms such as ^{4}He one must, instead, introduce a suitable model for $S(Q,\omega)$ and then evaluate the integral (6) explicitly by either a numerical or analytic method.

The dynamic structure factor of liquid ^{4}He differs from (8) in two respects: Firstly, as a result of recoil effects the center of the distribution is shifted to positive ω in accordance with the f-sum rule,

$$\int_{-\infty}^{\infty}\omega S(Q,\omega)d\omega=\omega_r, \tag{11}$$

where $\hbar\omega_r=(\hbar Q)^2/2m$ is the recoil energy, m being the atomic mass. Secondly, the distribution has a finite width and a shape that is charac-

teristic of the dynamics of the liquid. It is evident from Fig. 1 that recoil effects are important at large Q. On the other hand, the finite width of $S(Q,\omega)$ and its precise shape give a negligible contribution to the integral (6) for the present experimental conditions since the incident neutron energy (26.9 THz) is 2 orders of magnitude greater than either the roton energy (0.18 THz) or the average kinetic energy per atom (0.28 THz). Thus we may adopt the model

$$S(Q,\omega)=S(Q)\delta(\omega-\omega_r/S(Q)), \tag{12}$$

which satisfies both (2) and (11). Since the recoil term is important only at large Q where $S(Q)\simeq 1$, we replace $\omega_r/S(Q)$ by ω_r in evaluating the integral (6). It then follows that

$$\chi(\epsilon,\phi)=\eta(\epsilon-\omega_r)S(Q)\chi_0(\phi), \tag{13}$$

in which $Q=Q(\omega_r)$ so that

$$Q=k\left(\frac{2A}{A+1}\right)^{1/2}\left(1-\frac{\cos\phi}{A+1}[\cos\phi+(A^2-\sin^2\phi)^{1/2}]\right)^{1/2}, \tag{14}$$

where $A=m/m_n$ is the atom-to-neutron mass ratio. Finally, apart from a constant factor, $\chi_0(\phi)$ is the free-atom differential scattering cross section,

$$\chi_0(\phi)=\frac{A}{(A+1)^2}\frac{[\cos\phi+(A^2-\sin^2\phi)^{1/2}]^2}{(A^2-\sin^2\phi)^{1/2}}. \tag{15}$$

A comparison of the approximate result (13) with results obtained from a numerical evaluation of the integral (6) using a realistic model[40] for $S(Q,\omega)$ shows that the error in Eq. (13) is $\lesssim 0.5\%$ for the present experimental conditions.

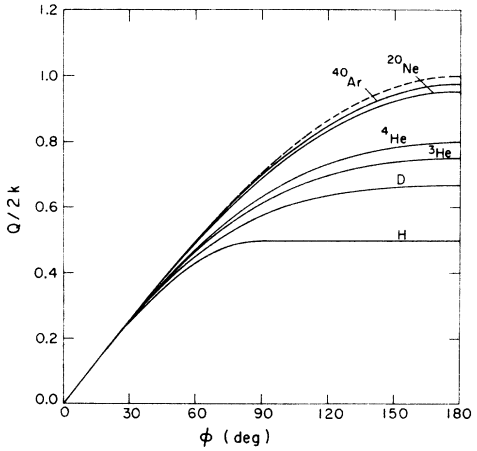

FIG. 2. Corrected wave vector as a function of the scattering angle for various values of the atomic mass. The dashed curve show the static wave vector Q_0 which corresponds to an infinite atomic mass.

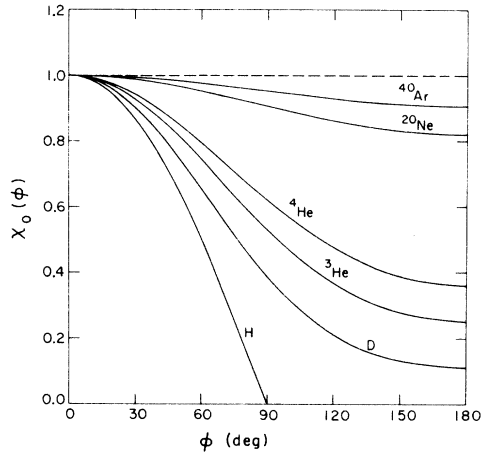

FIG. 3. Free-atom differential scattering cross section as a function of the scattering angle for various values of the atomic mass. The dashed line shows the result for an infinite atomic mass, i.e., for a rigidly bound atom.

Note that in the above treatment both the intensity and the wave vector are corrected for inelastic scattering effects. In the Placzek method,[38,39] on the other hand, only the intensity is corrected, since the latter method is based on an expansion about the static wave vector Q_0, and the intensity correction depends on the derivatives of $S(Q_0)$.

Figure 2 shows a comparison of Q for various values of A (solid curves) with the static wave vector Q_0 (dashed curve). A similar comparison for $\chi_0(\phi)$ is shown in Fig. 3. A selection of numerical values for the wave-vector correction Q_0-Q, the inelastic scattering correction $1-\chi_0(\phi)$, and the detector efficiency $\eta(\epsilon-\omega_r)$ are given in Table I for the present experimental conditions.

III. EXPERIMENT

The measurements were carried out using the triple-axis crystal spectrometer at the L3 experimental facility of the NRU reactor at the Chalk River Nuclear Laboratories. The analyzer crystal was removed so that the spectrometer could function as a conventional double-axis instrument. The scattering angle of the Be(110) monochromator planes (mosaic spread 0.3°) was chosen to be $2\theta_M=44.1°$ which gave an incident neutron energy $\hbar\epsilon=111.1$ meV. Thus $\epsilon/2\pi=26.87$ THz, which corresponds to a wave vector $k=7.323$ Å^{-1} and a wavelength $\lambda=2\pi/k=0.8581$ Å. At this wavelength the order contamination in the incident beam is negligible ($<1\%$) so that no filter was required. The scattered neutrons were detected with a ^{3}He proportional counter for which

TABLE I. Representative values of various quantities used in the corrections to determine $S(Q)$. The quantities are defined in the text.

Effect	Quantity	Q (Å^{-1}) 0.5	1.0	1.5	2.0	3.0	4.0	6.0	8.0	10.0
scattering angle	ϕ (deg)	4	8	12	16	25	33	51	73	103
wave-vector correction	$Q_0 - Q$ (Å^{-1})	0.01	0.01	0.01	0.02	0.04	0.08	0.26	0.66	1.48
inelastic scattering correction	$1-\chi_0(\phi)$ (%)	0	0	1	2	4	7	15	28	45
detector efficiency	$\eta(\epsilon-\omega_r)$ (%)	69	69	69	70	70	71	73	76	80
empty-cassette scattering [a]	C_0/C (%)	97	53	20	6	10	8	8	11	15
fast-neutron background [a]	C_f/C (%)	41	19	5	1	1	1	1	1	1
multiple scattering [a]	C_m/C_1 (%)	3	3	1	1	1	1	1	1	1

[a]Values for $T=4.27$ K.

the absorption efficiency at the incident neutron energy was 69%. The angular collimations between the monochromator and specimen and between the specimen and detector were 0.37° and 0.31°, respectively.

The liquid ^{4}He specimen was contained in a cylindrical aluminum cassette with its axis in the vertical direction and hence perpendicular to the plane of scattering. The cassette had an inner radius of 2.22 cm, a wall thickness of 0.025 cm and a length that exceeded the 5-cm beam height. The transmission of the specimen varied from 92% to 93% over the temperature range of the present experiments. Cadmium discs were suspended in the liquid at 0.74-cm intervals to help reduce multiple-scattering effects.

The cassette was connected through a large valve to the bottom of a ^{4}He reservoir which was contained in a metal cryostat. The temperature of the liquid ^{4}He was controlled to within 0.01 K by pumping on the reservoir and the temperature was determined by measuring the vapor pressure above the liquid. Measurements were carried out with the ^{4}He at 11 temperatures: 1.00, 1.38, 1.77, 1.97, 2.07, 2.12, 2.15, 2.27, 3.00, 3.60, and 4.27 K. At each temperature, the number of neutrons observed in the time required to accumulate a fixed number of counts in the incident beam monitor was recorded for scattering angles $1.0° \leq \phi \leq 124.0°$ in steps of 0.1°. The scattering with the cassette empty at 4.27 K was similarly determined for the same angles. During each scan, the fast-neutron background was measured, by automatically inserting a Boral and cadmium shutter in the incident beam to absorb the thermal neutrons for $1.0° \leq \phi \leq 20.0°$ in steps of 1.0° and at larger angles in steps of 10.0°. Except at low ϕ angles, the fast-neutron background was essentially independent of angle, but it did exhibit long-term variations with time due to changes in the loading of the reactor.

Figure 4 shows a selection of our results. The upper curve is the observed total scattering with helium in the cassette at 4.27 K. This corresponds to the quantity C in Eq. (16) below. The middle curve is the total scattering with the cassette empty (C_0) and the lower curve shows the fast-neutron backgrounds for both full (C_f) and empty (C_{0f}) conditions. The latter appear as a single curve on this scale since $C_{0f} \simeq C_f$.

The peaks in the two total-scattering spectra in Fig. 4 are the Debye-Scherrer peaks from the aluminum cassette. At first sight, these peaks might appear to present a serious problem but, as we shall see in the following section, they are actually an advantage, since they give a very sensitive indication of whether or not one has allowed correctly for the shielding of the cassette by the helium. Aluminum, being a very weak scatterer, is possibly the best material to use for the cassette in such a study. One could use

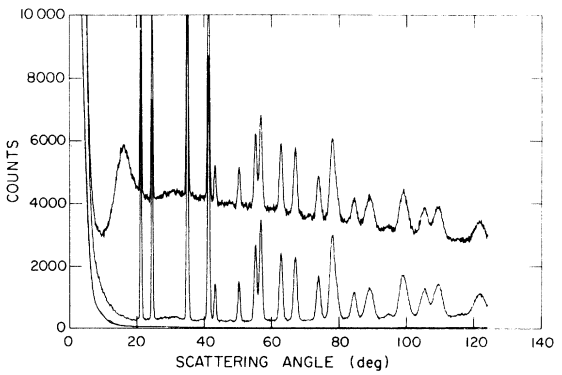

FIG. 4. Observed scattered-neutron distributions. The upper curve shows the total scattering with liquid ^{4}He at 4.27 K in the cassette, the middle curve the total scattering with the cassette empty at 4.27 K, and the lower curves the corresponding fast-neutron backgrounds. The latter appear as a single curve, since the fast-neutron background is, except at very small scattering angles, essentially the same for full and empty conditions.

a material with essentially zero coherent elastic scattering, and hence no Debye-Scherrer lines, but the level of the incoherent elastic scattering would then be considerably higher than the average level of the elastic scattering for aluminum. For example, for vanadium it would be about four times higher for the same wall thickness (which is largely determined by machining capabilities) and so comparable with the net scattering by the helium. This would lead to poorer average statistical accuracy as well as a possible systematic error because of the uncertainty about the shielding corrections. Note that the principal maximum in the ^{4}He scattering is well clear of any Debye-Scherrer lines and that a second weaker maximum is also apparent in the raw data.

IV. ANALYSIS

The first step in the analysis of the diffraction data is to determine the corrected single scattering C_1, which is given by

$$C_1 = [(C - C_f) - B(C_0 - C_{0f})]D/A - C_m - C_{oc} . \tag{16}$$

Here C denotes the number of counts observed in the time required to accumulate a fixed number of counts in the incident beam monitor when the cassette is full, C_0 is the corresponding number of counts for the empty cassette, and C_f and C_{0f} are the corresponding fast-neutron-background counts. The quantity B corrects for the shielding of the cassette by the helium and[41] A corrects for the shielding of the helium by itself and by the cassette. The factor D corrects for the distortion of the monitor count by the higher-order neutrons in the incident beam. Finally, C_m corrects for the multiple scattering and C_{oc} for the order contamination. The theoretical expressions for A, B, D, C_m, and C_{oc} are given in the Appendix.

Apart from effects of counting statistics and instrumental resolution,

$$C_1 = G\chi(\epsilon, \phi) , \tag{17}$$

where G is the normalization constant which is proportional to the density of the liquid and to the monitor setting. The root-mean-square fluctuation in C_1 due to the effect of counting statistics is given by

$$[C + C_f + B^2(C_0 + C_{0f})]^{1/2} D/A . \tag{18}$$

Combining Eqs. (13) and (17), we see that

$$S(Q) = C_1/G\eta(\epsilon - \omega_r)\chi_0(\phi) . \tag{19}$$

This is the basic relation for the experimental determination of the static structure factor in the present paper.

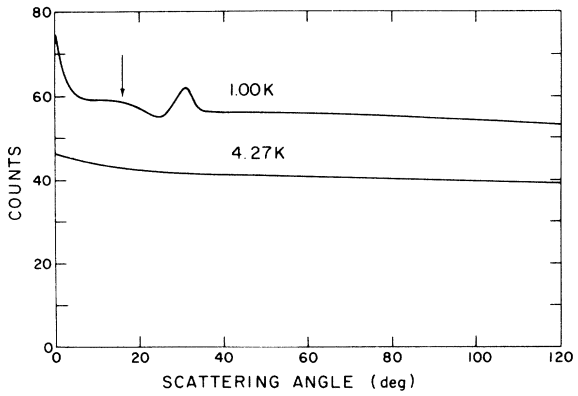

FIG. 5. Calculated multiple scattering at 1.00 and 4.27 K. The arrow denotes the position of the main diffraction maximum which has a corresponding corrected single scattering of 7631 counts at 1.00 K and 6023 counts at 4.27 K (see Fig. 6).

The values of the shielding factors A and B depend on the density of the liquid and hence on the temperature (see the Appendix). Thus, as the temperature varies from 1.00 to 4.27 K, A varies from 0.906 to 0.917 and B from 0.935 to 0.943. In the present experiment, order contamination is negligible so that we can put $D = 1$ and $C_{oc} = 0$. The calculated multiple scattering C_m is shown in Fig. 5 for two temperatures. The higher multiple scattering at the lower temperature is due primarily to the higher density. The structure in the multiple scattering at 1.00 K for $\phi < 40°$ is due to the presence of the sharp phonon-roton branch in $S(Q, \omega)$ which is absent above T_λ.

Figure 6 shows the corrected single scattering C_1 at 4.27 K which was obtained from Eq. (16) using the data shown in Fig. 4. The vertical lines indicate the positions of the Debye-Scherrer

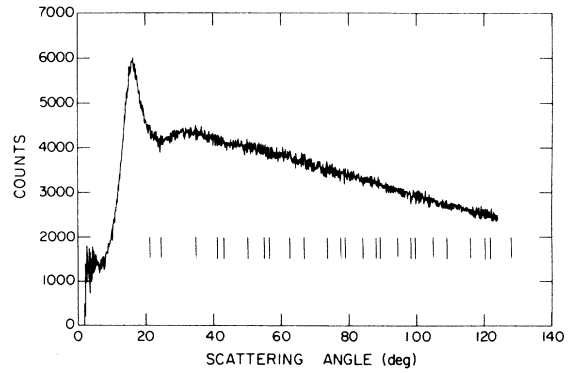

FIG. 6. Corrected single scattering at 4.27 K obtained from the data in Fig. 4 as described in the text. The vertical lines indicate the positions of the Debye-Scherrer peaks from the aluminum cassette.

peaks for the aluminum cassette. A small (≃1%) adjustment (with respect to the calculated value) in the value of the shielding factor B was necessary to make the effect of the Debye-Scherrer peaks vanish completely in C_1. The need for such an adjustment can easily be attributed to slight inhomogeneities in the incident beam and the fact that the cassette is not a "perfect" powder. The large statistical fluctuations in C_1 at small scattering angles are due to the fact that, in this region, C_0 and C are almost equal and the fast-neutron backgrounds are very large (see Fig. 4 and Table I).

The detector efficiency is of the form

$$\eta(\epsilon') = \eta(0)(1 - e^{-\lambda'/\lambda_c}), \tag{20}$$

where λ' is the wavelength corresponding to the scattered neutron energy $\hbar\epsilon'$ and

$$\lambda_c = \lambda_0/\rho_0\sigma_0 d. \tag{21}$$

Here ρ_0 is the ^{3}He number density in the detector, σ_0 is the absorption cross section per atom at the wavelength λ_0, and d is the thickness of the detector. The constant factor $\eta(0)$ can be absorbed into the normalization constant G in Eq. (19). For the detector used in the present experiments, $\lambda_c = 0.73$ Å.

The static structure factor $S(Q)$ was determined for each temperature from Eq. (19) with the normalization constant G chosen such that $S(Q) = 1$ at large Q. The results for the range $0.8 \leq Q \leq 10.8$ Å^{-1} are shown in Fig. 7. The results for $Q < 0.8$ Å^{-1} have large statistical uncertainties for reasons discussed above and hence have not been included. Above 0.8 Å^{-1}, groups of neighboring $S(Q)$ values were averaged to improve the statistical precision as much as was possible without significant loss of resolution. The final statistical precision of the $S(Q)$ results shown in Fig. 7 is, on the average, 0.8%. The residual systematic

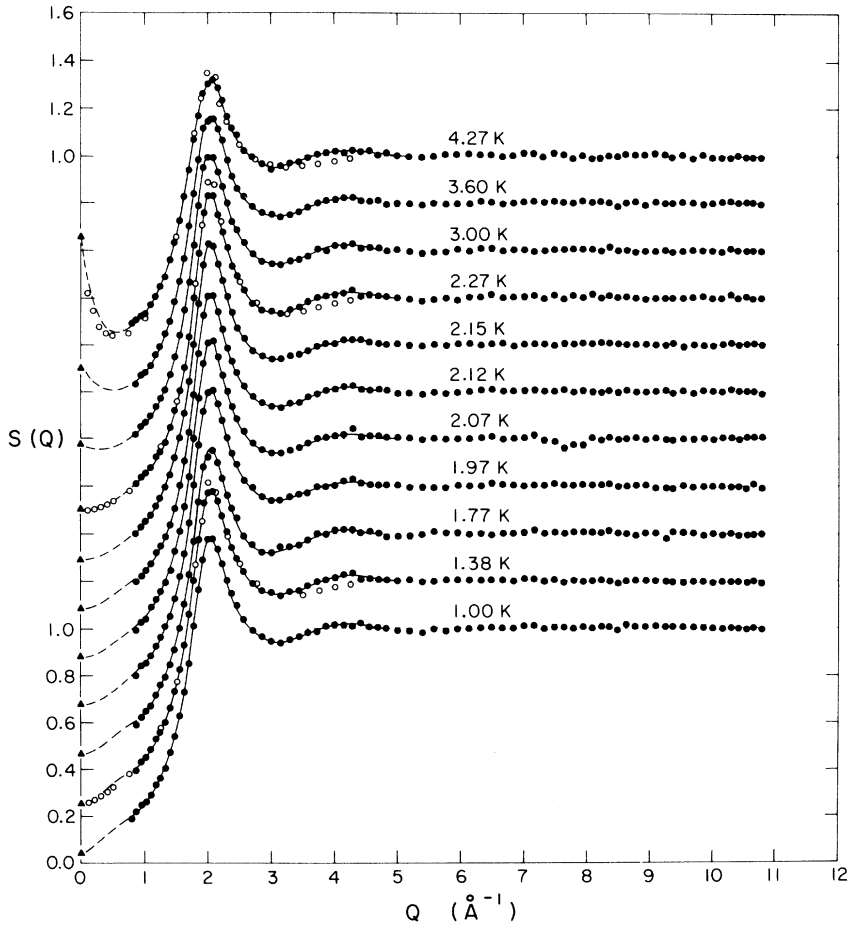

FIG. 7. Static structure factor of liquid ^{4}He at saturated vapor pressure for various temperatures. The filled circles show our present results, the open circles are the x-ray results of Gordon, Shaw, and Daunt (Ref. 9), the triangles denote the compressibility limit, the dashed curves were obtained from the small-angle x-ray-scattering results of Hallock (Ref. 12), and the solid curves were determined from a cubic-spline fit to our results.

error, which is due primarily to the approximations involved in the derivation of Eq. (13), is believed to be less than 1%. All other corrections (detector efficiency, multiple scattering, etc.) have an accuracy that is much better than 1%. The various corrections are summarized in Table I.

V. STATIC STRUCTURE FACTOR

Figure 7 shows a comparison of our present $S(Q)$ results (filled circles) with the earlier x-ray results of Gordon, Shaw, and Daunt[9] for temperatures of 1.4, 2.4, and 4.2 K (open circles). While there is approximate overall agreement between the two sets of measurements, our results for each temperature show a well-defined second maximum in $S(Q)$ near $Q = 4$ Å^{-1} which is absent in the x-ray results. The x-ray results also give somewhat larger values for the height of the main maximum.

The value of the static structure factor at $Q = 0$ is given by[42]

$$S(0) = \rho k_B T K_T , \tag{22}$$

where ρ is the number density and K_T the isothermal compressibility. Equivalently,

$$S(0) = \gamma k_B T / mc^2 , \tag{23}$$

TABLE II. Smoothed values of the static structure factor of liquid ^{4}He at 1.00 K. A complete listing of all our $S(Q)$ values, both smoothed and unsmoothed, is available in Ref. 45.

Q (Å^{-1})	$S(Q)$	Q (Å^{-1})	$S(Q)$
0.0	0.037	2.4	1.116
0.05	0.043	2.5	1.061
0.1	0.051	2.6	1.021
0.2	0.073	2.7	0.989
0.3	0.099	2.8	0.965
0.4	0.123	2.9	0.949
0.5	0.145	3.0	0.941
0.6	0.165	3.2	0.942
0.7	0.184	3.4	0.959
0.8	0.204	3.6	0.978
0.9	0.227	3.8	0.997
1.0	0.256	4.0	1.012
1.1	0.293	4.2	1.018
1.2	0.340	4.4	1.014
1.3	0.399	4.6	1.005
1.4	0.472	4.8	0.995
1.5	0.566	5.0	0.988
1.6	0.695	5.2	0.985
1.7	0.865	5.4	0.986
1.8	1.069	5.6	0.989
1.9	1.263	5.8	0.992
2.0	1.377	6.0	0.995
2.05	1.387	6.2	0.997
2.1	1.365	6.4	0.999
2.2	1.290	6.6	1.000
2.3	1.203	6.8	1.000

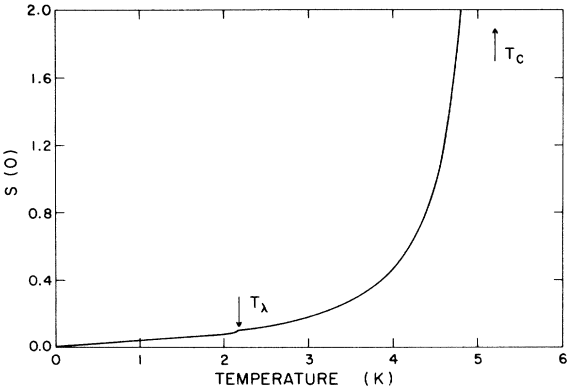

FIG. 8. Temperature dependence of $S(0)$ calculated from Eq. (23) with the help of the data for γ and c in Refs. 43 and 44. The arrows denote the position of the lambda point ($T_\lambda = 2.17$ K) and the critical point ($T_c = 5.20$ K).

where γ is the specific-heat ratio, m the atomic mass, and c the adiabatic sound velocity. The triangles in Fig. 7 show the values of $S(0)$ calculated from Eq. (23) using available data[43,44] for γ and c.

The dashed curves in Fig. 7 have been obtained by interpolating the small-angle x-ray-scattering

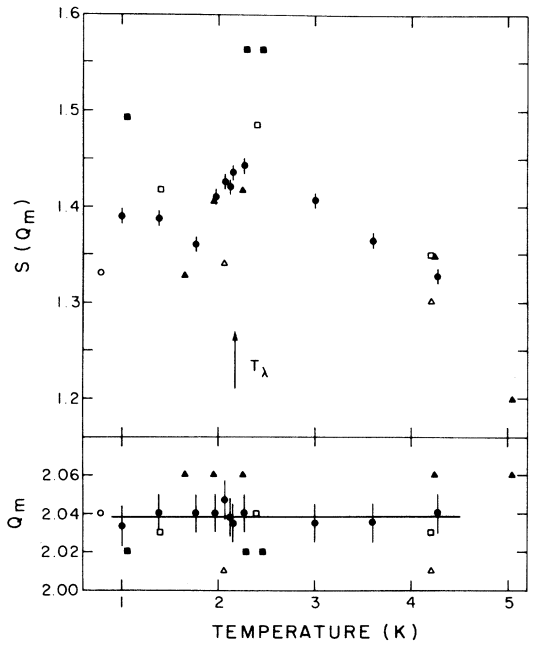

FIG. 9. Temperature dependence of the position Q_m and the height $S(Q_m)$ of the main maximum in the static structure factor of liquid ^{4}He. The filled symbols are obtained from neutron-diffraction measurements: present results (circles), Ref. 14 (triangles), Ref. 15 (squares). The open symbols are obtained from x-ray-diffraction measurements: Ref. 7 (triangles), Ref. 9 (squares), Ref. 10 (circle).

results of Hallock[12] which cover the range $0.133 \leq Q \leq 1.125$ Å^{-1}. These results are in good agreement with our present measurements in the region of overlap and with the compressibility limit.

Finally, the solid curves in Fig. 7 were obtained from our results by means of a cubic-spline-fitting program. These curves represent, in effect, the best smooth curves that are consistent with our $S(Q)$ results within the known statistical errors and which join smoothly onto the small-angle x-ray results. The smoothed $S(Q)$ values for $T = 1.00$ K are listed in Table II. A complete listing of the $S(Q)$ results for all temperatures, both smoothed and unsmoothed, is available in Ref. 45.

There are only two regions where $S(Q)$ shows any appreciable temperature dependence. The first is at small Q ($\lesssim 0.5$ Å^{-1}) where $S(Q)$ increases monotonically with increasing temperature. The temperature variation is strongest at $Q = 0$ where, as shown in Fig. 8, $S(0)$ diverges at the critical point T_c. The second region in which $S(Q)$ varies significantly with temperature is near the main diffraction maximum, $Q = Q_m$. It can be seen in the upper part of Fig. 9 that $S(Q_m)$ is largest near T_λ and decreases on both raising and lowering the temperature. The increase in $S(Q)$ on cooling from 4.27 K in the normal phase is a consequence of the increased spatial order of the atoms resulting from the increased density and the decreased thermal motion. Our results show clearly that the spatial order reaches a maximum at or near T_λ and then decreases on cooling in the superfluid phase. As discussed in Refs. 34–36, this decrease is an expected consequence of the Bose-Einstein condensation. This loss of spatial order on cooling through T_λ has also been clearly observed in a recent x-ray study by Robkoff *et al.*[46] and is also exhibited, though with somewhat less clarity, by the results of several of the earlier studies[9,14,15,17] which are also shown in Fig. 9. As we mentioned in the Introduction, there is clearly a large degree of scatter in the earlier results for $S(Q_m)$ and this was our main incentive for carrying out the present study. On the average, our new results are about an order of magnitude more accurate. The lower part of Fig. 9 shows that, to within our experimental uncertainties, the wave vector of the maximum is independent of temperature and has the value $Q_m = 2.04 \pm 0.01$ Å^{-1}. The earlier estimates are in reasonably good agreement with this value although, as was the case for $S(Q_m)$, they exhibit much more scatter than our new results.

Note that our results suggest a dip in $S(Q_m)$ at $T = 1.77$ K. The results of Hurst and Henshaw[14] (solid triangles) which, among the earlier results, agree best with our new values are also consistent with such behavior. This dip should, however, be checked by further measurements and should not, at present, be considered to be a well-established feature.

TABLE III. Values of the pair correlation function of liquid ^{4}He at 1.00 K. A complete listing of all our $g(r)$ values is available in Ref. 45.

r (Å)	$g(r)$	r (Å)	$g(r)$
2.0	0.001	5.0	0.892
2.1	0.013	5.2	0.879
2.2	0.043	5.4	0.886
2.3	0.105	5.6	0.910
2.4	0.190	5.8	0.942
2.5	0.305	6.0	0.976
2.6	0.449	6.2	1.006
2.7	0.598	6.4	1.029
2.8	0.757	6.6	1.042
2.9	0.916	6.8	1.047
3.0	1.061	7.0	1.045
3.1	1.183	7.2	1.037
3.2	1.277	7.4	1.025
3.3	1.339	7.6	1.011
3.4	1.371	7.8	0.998
3.5	1.377	8.0	0.987
3.6	1.363	8.2	0.979
3.7	1.334	8.4	0.976
3.8	1.296	8.6	0.977
3.9	1.253	8.8	0.982
4.0	1.208	9.0	0.988
4.2	1.123	9.2	0.995
4.4	1.046	9.4	1.002
4.6	0.979	9.6	1.007
4.8	0.927	9.8	1.010
		10.0	1.011

VI. PAIR CORRELATION FUNCTION

The static structure factors obtained as described in the previous sections have been Fourier analyzed via Eq. (3) to determine the corresponding pair correlation functions $g(r)$. Our values for $T = 1.00$ K are listed in Table III. A complete listing of our $g(r)$ values for all temperatures can be found in Ref. 45.

The method of analysis is illustrated in Fig. 10. The solid curve shows the smoothed $S(Q)$ distribution for 3.60 K obtained as described in Sec. V. The corresponding $g(r)$ curve obtained by a numerical integration of Eq. (3) is shown by the solid curve in the inset part of the figure. The variation in this latter curve for $r \lesssim 2$ Å^{-1} is a spurious effect caused by the fact that the quantity being Fourier analyzed is $Q[S(Q) - 1]$ rather than $S(Q)$ itself, and the quantity so obtained is $r[g(r) - 1]$ rather than $g(r)$. The errors in $S(Q)$

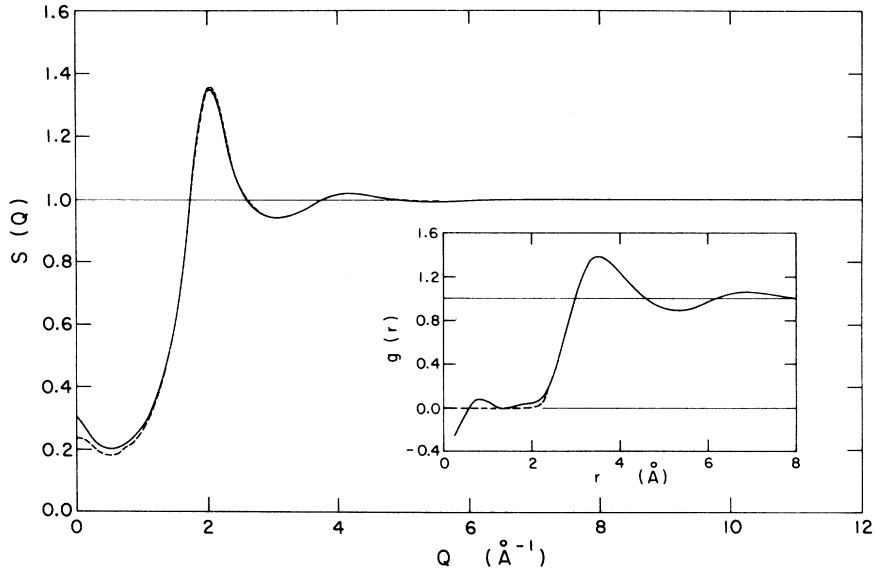

FIG. 10. Static structure factor $S(Q)$ of liquid ^{4}He at 3.60 K and the corresponding pair correlation function, $g(r)$ (inset). The dashed curves illustrate the degree of self-consistency of $S(Q)$ and $g(r)$ as discussed in the text.

at large Q are thus greatly amplified in the analysis and this leads to an enhancement of the errors in $g(r)$ at small r. In fact, $g(r)$ must be essentially zero when $r \lesssim 2$ Å^{-1} because of the strong hard-core repulsion of the atoms in this region. We thus adjust $g(r)$ as indicated by the dashed curve in the inset part of Fig. 10, and when we then perform the inverse Fourier transformation we obtain the dashed $S(Q)$ distribution. The latter agrees with our original distribution within 0.5% for $Q > 1$ Å^{-1} which is consistent with our earlier estimate of the size of the possible systematic error in our $S(Q)$ results. Thus, to within the experimental uncertainty, our $S(Q)$ results are consistent with the requirement that the corresponding $g(r)$ vanish inside the core of the interatomic potential. [The deviation of the dashed $S(Q)$ curve from the correct solid curve at small Q is simply a consequence of the truncation of $g(r)$ at large r in performing the inverse Fourier transform.]

Figure 11 shows a comparison of our results for $g(r)$ at 1.38 K (solid curve) with those obtained from x-ray diffraction[9] at 1.4 K (dashed curve). Note that the spurious oscillations in $g(r)$ at small r are very much larger in the x-ray results and that there are also substantial differences at larger r. The main discrepancy in

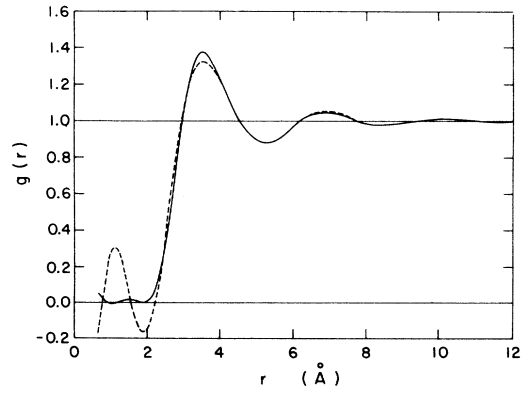

FIG. 11. Comparison of our present results for the pair correlation function of liquid ^{4}He at 1.38 K (solid curve) with those obtained by Gordon, Shaw, and Daunt (Ref. 9) from x-ray-diffraction measurements at 1.4 K (dashed curve).

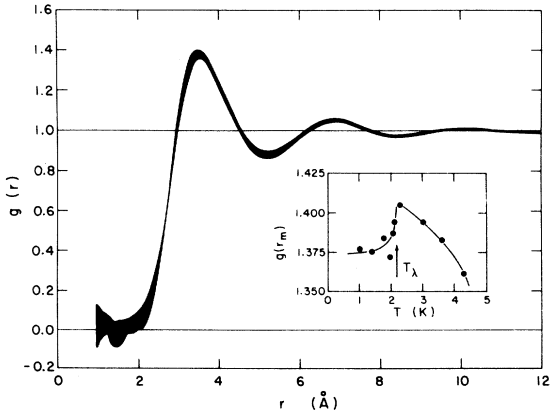

FIG. 12. Temperature variation of the pair correlation function of liquid ^{4}He between 1.00 and 4.27 K. The $g(r)$ results for all 11 temperatures lie within the solid band. The temperature variation at the main maximum is shown by the inset part of the figure.

the corresponding $S(Q)$ distributions (Fig. 7) is the presence of the weak secondary maximum in our results near $Q = 4$ Å^{-1} which was not observed in the x-ray measurements. We see clearly that, as expected, one must have good accuracy in $S(Q)$ at large Q in order to obtain good accuracy in $g(r)$ at small r.

When we plot our $g(r)$ distributions for the 11 different temperatures on the same graph we find that they all lie within the solid band shown in Fig. 12. Aside from the spurious variations at low r, the largest temperature variation in $g(r)$ occurs at the main maximum where it amounts to only about 4%. The temperature variation of this maximum is shown in the inset part of the figure. The position of the maximum in $g(r)$ is independent of temperature and has the value $r_m = 3.47 \pm 0.03$ Å.

As was the case for $S(Q_m)$ (Fig. 9), the variation of $g(r_m)$ also shows (and even more directly) that the spatial correlations of the atoms increase on cooling in the normal phase, reach a maximum at or near T_λ, and then decrease on cooling in the superfluid phase. The latter behavior reflects the fact that when atoms condense into the zero-momentum state they effectively no longer contribute to the spatial correlations of the atoms which give rise to the oscillations in $g(r)$. Note that $g(r_m)$ exhibits a typical "order-parameter" type of variation with temperature in the superfluid phase. As mentioned in the Introduction, a method for obtaining the condensate fraction $n_0(T)$ in superfluid ^{4}He from the temperature variations of $g(r)$ at large r was proposed[34,35] several years ago. Following this method, values of $n_0(T)$ for seven temperatures in the superfluid

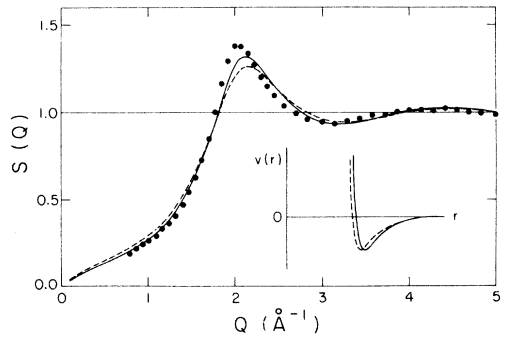

FIG. 13. Comparison of our unsmoothed results for $S(Q)$ at 1.00 K (circles) with the results of variational calculations by Chang and Campbell (Ref. 27) for $T = 0$. The dashed curve is calculated for the Lennard-Jones potential and the solid curve for the MDD-2 potential of Bruch and McGee (Ref. 48). These potentials are shown in the inset part of the figure. Both calculations employ the same Jastrow form for the ground-state wave function.

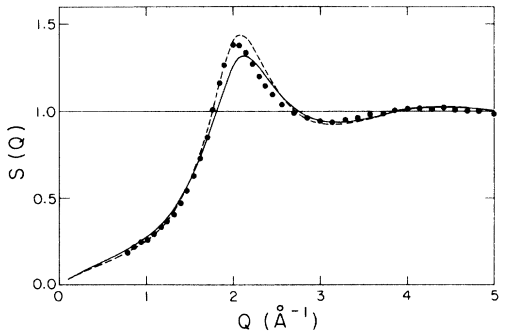

FIG. 14. Comparison of our unsmoothed results for $S(Q)$ at 1.00 K (circles) with the results of variational calculations by Chang and Campbell (Ref. 27) for $T = 0$. The solid curve is based on the Jastrow form for the ground-state wave function while the dashed curve includes three-body factors as well. Both calculations employ the MDD-2 model for the pair potential.

phase have been obtained[47] from the present results for $g(r)$ in the range $r \gtrsim 6$ Å.

VII. COMPARISON WITH THEORY

In the past 15 years, following the pioneering work of McMillan,[18] there have been many variational calculations[19-29] of $g(r)$ and $S(Q)$ at $T = 0$. Most of this work is based on the Lennard-Jones model for the interatomic pair potential. The parameters in the assumed ground-state wave function ψ are determined by minimizing the energy integral, and the pair correlation function is then obtained by integrating $|\psi|^2$ over the positions of all but two of the atoms. The various calculations differ both in the detailed form assumed for ψ and in the numerical and analytical techniques used to evaluate the many-dimensional integrals which occur. However, they all yield rather similar results for $g(r)$ and $S(Q)$, the discrepancies being $\lesssim 10\%$.

In the present article we shall confine our attention to the recent work of Chang and Campbell[27] which, we believe, is representative of the best of the variational calculations. Figures 13 and 14 show a comparison of some of their results for $S(Q)$ with our measurements at 1.00 K. In Fig. 13 the wave function is taken to be a Jastrow-type product of two-body factors. The dashed curve is then obtained for the Lennard-Jones potential and the solid curve for the Morse dipole-dipole (MDD-2) potential of Bruch and McGee.[48] Although the latter potential leads to better agreement with our results, the main peak is in both cases lower in intensity and at a larger wave vector than is observed. In Fig. 14 the calculated curves are both based on the MDD-2 potential

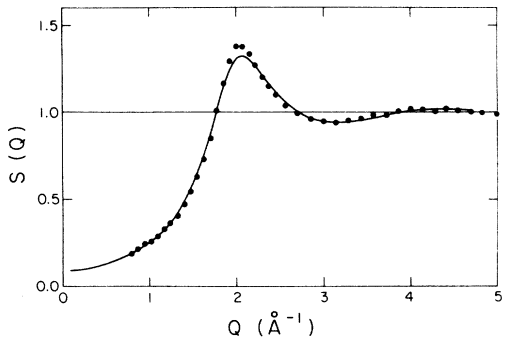

FIG. 15. Comparison of our unsmoothed results for $S(Q)$ at 1.00 K (circles) with the results of Monte Carlo calculations by Whitlock *et al.* (Ref. 30) for $T=0$. The calculations are based on the Lennard-Jones model for the pair potential.

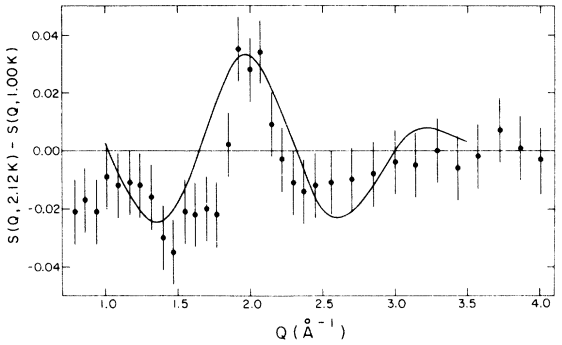

FIG. 17. Temperature change of our $S(Q)$ results between 2.12 and 1.00 K (circles). The solid curve is the result of the theoretical calculation by De Michelis *et al.* (Ref. 32) of the change between $T=0$ and 2.1 K.

but differ in the structure of the wave function. The solid curve employs the Jastrow form for ψ while the dashed curve includes three-body factors as well. The effect of the latter is to improve the agreement with experiment but significant discrepancies remain.

An alternative approach to the theoretical calculation of $g(r)$ and $S(Q)$ is based on a direct numerical integration of the many-body Schrödinger equation.[26,30] Here one considers a finite but reasonably large number of atoms (e.g., 256) in a region of space whose dimensions are determined by the density of interest. With periodic boundary conditions, the Schrödinger equation is first transformed to an integral equation by the standard Green's-function method and the latter equation is then solved numerically with the help of a Monte Carlo algorithm. The advantage of this method is that, for a given model of the interatomic potential, the accuracy of the final results is in principle limited only by statistical sampling errors. At present, results obtained by this method are available for both the hard-sphere[26] and Lennard-Jones[30] potentials.

The calculations of Whitlock *et al.*[30] using the latter potential give the $S(Q)$ and $g(r)$ curves shown in Figs. 15 and 16, respectively. The agreement with our results is certainly much better than for any of the variational calculations. There are, however, still significant discrepancies as regards the heights and, to a lesser extent, the widths of the principal peaks. These discrepancies can probably be attributed to the inadequacy of the Lennard-Jones pair potential. It is not clear, however, whether one simply needs to use a better pair potential or if it is also necessary to include many-body forces. As one can see from the curves in Fig. 13, the discrepancies in Fig. 15 are very similar in size to the differences that can result from using different pair potentials. Although our earlier attempt[33] to determine the effective pair potential in liquid ^{4}He directly from neutron-inelastic-scattering data did not give a unique result, it did indicate that none of the commonly used pair potentials (e.g., Lennard-Jones, Buckingham, and Morse) was adequate and that many-body forces were probably very important.

It seems very improbable that the differences between theory and experiment can be attributed to the fact that the calculations are for $T=0$ while the experimental results are for $T=1.00$ K. One would expect, and our new results certainly suggest (see, e.g., Figs. 9 and 12), that there will be little change in $S(Q)$ and $g(r)$ below 1.00 K. At present, the most we can conclude is that the experimentally determined $S(Q)$ and $g(r)$ imply that a somewhat greater degree of spatial order is present in liquid ^{4}He than should be present if

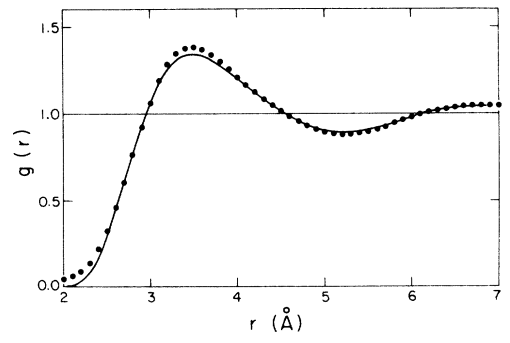

FIG. 16. Comparison of our results for $g(r)$ at 1.00 K (circles) with the results of Monte Carlo calculations by Whitlock *et al.* (Ref. 30) for $T=0$. The calculations are based on the Lennard-Jones model for the pair potential.

the atoms interacted via additive forces of the Lennard-Jones type.

De Michelis *et al.*[32] have recently presented the results of a calculation of the temperature variation of $S(Q)$ due to the thermal excitation of rotons out of a Jastrow ground state. Their results for the change in $S(Q)$ between $T=0$ and 2.1 K are shown by the curve in Fig. 17 which is seen to be in reasonably good agreement with our values for the change in $S(Q)$ between 1.00 and 2.12 K. To the extent that the calculations are correct, this agreement is further evidence that $S(Q)$ changes very little below 1.0 K.

VIII. CONCLUSIONS

In this paper we have presented new results for $S(Q)$ for liquid ^{4}He at saturated vapor pressure covering a wide range of wave vectors ($0.8 \leq Q \leq 10.8$ Å^{-1}) and temperatures ($1.00 \leq T \leq 4.27$ K). The values are, in general, much more accurate than those obtained in the numerous earlier studies, and this accuracy has been achieved by applying improved correction procedures to raw data having high statistical accuracy and obtained under conditions of good experimental resolution. These new results show a weak but well-defined second maximum at each temperature. We have also effectively reached the infinite-Q limit since the oscillations in $S(Q)$ have died out beyond about 6 Å^{-1}. Combining our values with the values of $S(Q)$ known from thermodynamic measurements and Hallock's[12] very precise values for $0.133 \leq Q \leq 1.125$ Å^{-1} gives essentially a complete picture of $S(Q)$ for each of the 11 temperatures.

The achievement of the infinite-Q limit has allowed us to obtain a very accurate normalization of $S(Q)$ and also, in inverting $S(Q)$ to obtain $g(r)$, to avoid the usual truncation errors so that the spurious oscillations in our $g(r)$ at small r are much smaller than in earlier studies. To well within the estimated errors, self-consistency between $S(Q)$ and $g(r)$ is obtained when one requires that $g(r)$ be zero for small r.

The variations with temperature of both $S(Q)$ and $g(r)$ show clearly that the degree of spatial order in liquid ^{4}He increases on cooling in the normal phase, reaches a maximum at or near $T_\lambda = 2.17$ K, and then decreases on cooling in the superfluid phase. This reversal is undoubtedly a consequence of the Bose-Einstein condensation.

Our new results for $S(Q)$ and $g(r)$ are sufficiently accurate to provide critical tests of the excellent theoretical calculations that have appeared in recent years. On detailed comparison, we find that the results for $S(Q)$ and $g(r)$ obtained by Whitlock *et al.*[30] by direct Monte Carlo integration of the Scrhödinger equation are in substantially better agreement with experiment than the results given by any of the numerous variational calculations. They still, however, underestimate the heights and overestimate the widths of the principal peaks in $S(Q)$ and $g(r)$. There thus appears to be a greater degree of spatial order in liquid ^{4}He than the calculations indicate there would be if the atoms interacted via additive central forces of the Lennard-Jones type. We feel that the calculations can most readily be improved by using more realistic interatomic interactions, and we hope that the results presented here will encourage further calculations not only for $T=0$, but for finite temperatures as well.

ACKNOWLEDGMENTS

The valuable technical assistance of D. C. Tennant and H. F. Nieman is gratefully acknowledged.

APPENDIX

In this Appendix we discuss the calculation of the correction terms in Eq. (16). In general, the shielding factors A and B depend on the scattering angle ϕ and on the size and shape of the specimen container. In particular, for the cylindrical cassette employed in the present experiments, they depend on the dimensionless variables Σr and $\Sigma_c t$, where r is the radius and t the wall thickness of the cassette, $\Sigma = \rho\sigma$ is the total cross section per unit volume of the liquid (i.e., the inverse mean free path), where ρ is the number density and σ the total cross section per atom, and Σ_c is the corresponding quantity for the cassette.

For situations such as those that occur typically in x-ray diffraction where Σr and $\Sigma_c t$ are $\gtrsim 1$, the expressions for A and B are extremely complex,[49] especially when the incident beam is narrower than the cassette.[50] However, in the present experiments where $\Sigma r \simeq 0.05$ and $\Sigma_c t \simeq 0.003$ and where the incident beam is slightly wider than the cassette, we can use the series expansions[51]

$$A = \begin{cases} 1 - (8/\pi)(\frac{2}{3}\Sigma r + \Sigma_c t) + \frac{3}{2}(\Sigma r)^2 + \cdots & (\phi = 0), \\ 1 - (8/\pi)(\frac{2}{3}\Sigma r + \Sigma_c t) + 2(\Sigma r)^2 + \cdots & (\phi = \pi), \end{cases} \tag{A1}$$

and

$$B = \begin{cases} 1 - (4/\pi)(\Sigma r) + (\Sigma r)^2 + \cdots & (\phi = 0), \\ 1 - (4/\pi)(\Sigma r) + 2(\Sigma r)^2 + \cdots & (\phi = \pi). \end{cases} \tag{A2}$$

The advantage of a cylindrical cassette is that the ϕ dependence of A and B enters only in second

order. Since $(\Sigma r)^2 \simeq 0.0025$ we can, for all practical purposes, neglect the ϕ dependence and simply use average values for A and B.

The monitor-distortion factor is

$$D = \sum_{n=1}^{\infty} \frac{1}{n}\left(\frac{I_n}{I_1}\right), \tag{A3}$$

where I_n/I_1 is the ratio of the nth-order flux to the first-order flux in the incident beam, and the order-contamination term is given by

$$C_{oc} = G \sum_{n=2}^{\infty} \left(\frac{I_n}{I_1}\right) \chi(n^2\epsilon, \phi), \tag{A4}$$

where G is the normalization constant in Eq. (17).

The multiple-scattering correction is

$$C_m = G\Delta\chi_2(\epsilon, \phi), \tag{A5}$$

where Δ is the multiple-scattering ratio[52] which depends somewhat on the density but is typically of the order of 0.02 for the present experiment conditions. Finally,

$$\chi_2(\epsilon, \phi) = \int_0^{\infty} \eta(\epsilon') \frac{k'}{k} R_2(\vec{k}, \vec{k}') d\epsilon', \tag{A6}$$

in which $R_2(\vec{k}, \vec{k}')$ is the double-scattering function.[52] This latter quantity is an integral over a product of $S(Q, \omega)$'s, one for each collision, and is evaluated numerically with the help of an empirical model for $S(Q, \omega)$ as described in Ref. 40.

*Present address: Atomic Energy of Canada Limited Research Company, 275 Slater St., Ottawa, Ontario, Canada K1A 1E5.

[1]W. H. Keesom and K. W. Taconis, Physica 4, 28, 256 (1937); 5, 270 (1938).
[2]J. Reekie, Proc. Cambridge Philos. Soc. 36, 236 (1940); 43, 262 (1947).
[3]J. Reekie, T. S. Hutchison, and C. F. A. Beaumont, Proc. Phys. Soc. London A66, 409 (1953).
[4]J. Reekie and T. S. Hutchison, Phys. Rev. 92, 827 (1953).
[5]A. G. Tweet, Phys. Rev. 93, 15 (1954).
[6]W. L. Gordon, C. H. Shaw, and J. G. Daunt, Phys. Rev. 96, 1444 (1954).
[7]C. F. A. Beaumont and J. Reekie, Proc. R. Soc. London, Ser. A 228, 363 (1955).
[8]L. Goldstein and J. Reekie, Phys. Rev. 98, 857 (1955).
[9]W. L. Gordon, C. H. Shaw, and J. G. Daunt, J. Phys. Chem. Solids 5, 117 (1958).
[10]E. K. Achter and L. Meyer, Phys. Rev. 188, 291 (1969).
[11]R. B. Hallock, Phys. Rev. Lett. 23, 830 (1969).
[12]R. B. Hallock, Phys. Rev. A 5, 320 (1972).
[13]D. G. Henshaw and D. G. Hurst, Phys. Rev. 91, 1222 (1953).
[14]D. G. Hurst and D. G. Henshaw, Phys. Rev. 100, 994 (1955).
[15]D. G. Henshaw, Phys. Rev. 119, 9 (1960).
[16]D. G. Henshaw, Phys. Rev. 119, 14 (1960).
[17]B. Mozer, L. A. De Graaf, and B. Le Neindre, Phys. Rev. A 9, 448 (1974); R. D. Mountain and H. J. Raveché, J. Res. Nat. Bur. Stand. 77A, 725 (1973).
[18]W. L. McMillan, Phys. Rev. 138, A442 (1965).
[19]W. E. Massey, Phys. Rev. 151, 153 (1966).
[20]D. Schiff and L. Verlet, Phys. Rev. 160, 208 (1967).
[21]W. E. Massey and C. W. Woo, Phys. Rev. 164, 256 (1967).
[22]C. E. Campbell and E. Feenberg, Phys. Rev. 188, 396 (1969).
[23]W. P. Francis, G. V. Chester, and L. Reatto, Phys. Rev. A 1, 86 (1970).
[24]R. D. Murphy and R. O. Watts, J. Low Temp. Phys. 2, 507 (1970).
[25]R. D. Murphy, Phys. Rev. A 5, 331 (1972).
[26]M. H. Kalos, D. Levesque, and L. Verlet, Phys. Rev. A 9, 2178 (1974).
[27]C. C. Chang and C. E. Campbell, Phys. Rev. B 15, 4238 (1977).
[28]C. De Michelis, G. Masserini, and L. Reatto, Phys. Rev. A 18, 296 (1978).
[29]S. Chakravarty and N. W. Ashcroft, Phys. Rev. B 18, 2978 (1978).
[30]P. A. Whitlock, D. M. Ceperley, G. V. Chester, and M. H. Kalos, Phys. Rev. B 19, 5598 (1979).
[31]T. Samulski and A. Isihara, Physica 86A, 257 (1977).
[32]C. De Michelis, G. L. Masserini, and L. Reatto, Phys. Lett. 66A, 484 (1978).
[33]V. F. Sears, A. D. B. Woods, E. C. Svensson, and P. Martel, *Proceedings of the International Conference on Neutron Inelastic Scattering, 1977* (IAEA, Vienna, 1978), Vol. II, p. 23.
[34]G. J. Hyland, G. Rowlands, and F. W. Cummings, Phys. Lett. 31A, 465 (1970).
[35]F. W. Cummings, G. J. Hyland, and G. Rowlands, Phys. Kondens. Mater. 12, 90 (1970).
[36]H. J. Raveché and R. D. Mountain, Phys. Rev. A 9, 435 (1974).
[37]W. Marshall and S. W. Lovesey, *Theory of Thermal Neutron Scattering* (Clarendon, Oxford, 1971).
[38]J. L. Yarnell, M. J. Katz, R. G. Wenzel, and S. H. Koenig, Phys. Rev. A 7, 2130 (1973).
[39]G. Placzek, Phys. Rev. 86, 377 (1952).
[40]V. F. Sears, Nucl. Instrum. Methods 123, 521 (1975).
[41]The shielding factor A is not to be confused with the atom-to-neutron mass ratio (Sec. II) which is also conventionally denoted by A.
[42]P. J. Price, Phys. Rev. 94, 257 (1954).
[43]R. D. McCarty, J. Phys. Chem. Ref. Data 2, 923 (1973).
[44]J. S. Brooks and R. J. Donnelly, J. Phys. Chem. Ref. Data 6, 51 (1977).
[45]V. F. Sears, E. C. Svensson, A. D. B. Woods, and P. Martel, Atomic Energy of Canada Limited Report No. AECL-6779, 1979.
[46]H. N. Robkoff, D. A. Ewen, and R. B. Hallock, Phys. Rev. Lett. 43, 2006 (1979).
[47]V. F. Sears and E. C. Svensson, Phys. Rev. Lett. 43, 2009 (1979).
[48]L. W. Bruch and I. J. McGee, J. Chem. Phys. 46, 2959 (1967); 52, 5884 (1970).
[49]H. H. Paalman and C. J. Pings, J. Appl. Phys. 33, 2635 (1962).
[50]A. P. Kendig and C. J. Pings, J. Appl. Phys. 36, 1692 (1965).
[51]V. F. Sears (unpublished).
[52]V. F. Sears, Adv. Phys. 24, 1 (1975).